

# Effect of Solution Heat Treatments on the Microstructure and Mechanical Properties of a Die-Cast AlSi7MgMn Alloy

GIULIO TIMELLI, OTTO LOHNE, LARS ARNBERG, and HANS IVAR LAUKLI

The influence of solution heat treatment time and temperature on the microstructure and mechanical properties and the mode of fracture of a high-pressure die-cast AlSi7MgMn alloy is reported. Metallographic and image analysis techniques have been used to quantitatively examine the microstructural changes occurring during solution heat treatment. A solution heat treatment of 15 minutes at 475 °C, or even more at 525 °C, is sufficient to spheroidize the eutectic Si, as well as coarsen and increase the interparticle distance of the eutectic Si. Increasing the solutionizing temperature from 475 °C to 525 °C improves the mechanical properties.

DOI: 10.1007/s11661-008-9527-0

© The Minerals, Metals & Materials Society and ASM International 2008

## I. INTRODUCTION

HIGH-PRESSURE die casting (HPDC) is an efficient and economical process. When used to its maximum potential, an aluminum die-cast component may replace an assembly composed of a variety of parts produced by, for example, extrusion. Consolidation into a single die casting can significantly reduce cost and labor.<sup>[1-4]</sup> While high velocity allows for the production of thin-walled castings, the associated turbulent conditions remain the major source of interior and surface casting defects, which may have deleterious effects on the mechanical properties.<sup>[5,6]</sup> Defect-containing regions in a tensile sample reduce the load-bearing area and, therefore, produce a concentration of the strain. Castings with thin sections, such as those produced by HPDC technology, are vulnerable to the effect of defects, because a single macrodefect can cover a significant fraction of the cross-sectional area. Defects, commonly found in conventional die-cast components, are porosity, due mainly to the entrapment of gases such as air, nitrogen, hydrogen, or vapors formed by the decomposition of organic die-wall lubricants.<sup>[1-4,7-9]</sup> These pores, particularly those located close to the casting surface, may expand during conventional solution heat treatment, which results in unacceptable surface blisters. Therefore, the application of aluminum die castings is often limited to nonstructural components that do not require this type of heat treatment. New technical evolutions of the traditional HPDC process, such as vacuum technique, pore-free, and semisolid

processes, lead to the production of high-integrity thin-walled castings.<sup>[1-4]</sup> However, recent work has revealed a process window in which HPDC components may be heat treated without encountering blistering phenomena.<sup>[7-9]</sup> This refers to a general reduction in the solution heat treatment cycle, which also influences productivity and the manufacturing cost.

Various efforts have been made to investigate the effect of solution temperature and time on the microstructure and mechanical properties of gravity-cast AlSiMg alloys.<sup>[10-16]</sup> It was established that the magnesium and silicon contents in  $\alpha$ -Al phase reach the maximum equilibrium level according to the alloy composition, and that the distribution of magnesium and silicon becomes homogeneous within less than 1 hour of solution heat treatment. The mathematical model proposed by Rometsch *et al.* also provides evidence that the dissolution of the primary Mg<sub>2</sub>Si particles and the homogenization of the  $\alpha$ -Al solid solution are strongly influenced by the scale of the microstructure.<sup>[11]</sup>

It has been reported that solution heat treatment changes the morphology of eutectic silicon from a polyhedral to a globular structure and that the kinetics of spheroidization and coarsening processes occur much more rapidly in the modified structure.<sup>[10,12,13]</sup> These microstructural transformations (to some extent) have an effect on the ductility of the alloy, *i.e.*, they increase the fracture strain, as they make it more difficult for the silicon particles to fracture.<sup>[17-21]</sup>

In this study, the combined effect of the solution temperature (475 °C and 525 °C) and the time (in the range of 15 to 480 minutes) on the microstructure, tensile properties, hardness, and fracture mode of a Sr-modified die-cast AlSi7MgMn alloy was investigated. A comparison between a short (15 to 60 minutes) and prolonged solution heat treatment (240 to 480 minutes) was then carried out; this described how the aluminum alloy die castings may be solution heat treated at high temperature without encountering problems with blistering.

GIULIO TIMELLI, Postdoctoral Student, is with the Department of Management and Engineering, University of Padova, I-36100 Vicenza, Italy. Contact e-mail: timelli@gest.unipd.it OTTO LOHNE and LARS ARNBERG, Full Professors, are with the Department of Material Science and Technology, Norwegian University of Science and Technology, N-7491 Trondheim, Norway. HANS IVAR LAUKLI, Principal Engineer, is with the Hydro Aluminium Products, Research & Technology Development, N-6601 Sunndalsøra, Norway.

Manuscript submitted November 12, 2007.

Article published online April 26, 2008

## II. EXPERIMENTAL METHODS

In the present work, a primary AlSi7MgMn foundry alloy has been used. The chemical composition, measured on separately poured samples, is shown in Table I. The liquidus temperature of the alloy was determined by the solidification model program Alstruc (SINTEF, Trondheim, Norway),<sup>[22]</sup>  $T_{liq} = 617$  °C. Key elements in addition to silicon and the modifying strontium are manganese and magnesium. The Fe content was kept below 0.14 wt pct, to minimize the formation of the iron-rich  $\beta$ -phase,  $Al_3FeSi$ , which normally appears as a needlelike shape in the cast microstructure. The morphology of Fe-bearing needles deteriorates the strength and ductility behavior and promotes the initiation of cracks under load.<sup>[23]</sup> In place of Fe, manganese is used to provide good ejection behavior and reduced die soldering. Zovi *et al.*<sup>[24]</sup> showed that, with an Fe content below 0.15 wt pct, the ejection behavior improves with the addition of Mn and that, at levels exceeding 0.4 wt pct, the desired behavior appears. Magnesium determines here the yield strength (YS), ultimate tensile strength (UTS), and aging behavior of the alloy.

Cast-to-shape specimens were produced using a multicavity die in Hydro Aluminium's Bühler SC42D cold chamber die-casting machine (Bühler Druckguss AG, Uzwil, Switzerland) with a locking force of 4.1 MN. The die that was used enabled two cylindrical tensile specimens and plates and one Charpy V-notch specimen to be cast from each shot. A detailed description of the HPDC machine, the casting procedure, and the process parameters is given elsewhere.<sup>[25,26]</sup> Briefly, 15 to 20 castings were scrapped after the startup, to reach a quasi-steady-state temperature in the shot chamber and die. Oil circulation channels in the die served to stabilize the temperature (at ~200 °C). Table II summarizes the process parameters that guarantee high-integrity die castings. By means of a dynamic shot control system in the HPDC machine, every casting was documented with its shot profile, to monitor the final quality and repeatability.

The investigated cylindrical tensile specimens had a total length of 125 mm, a gage length of 32.5 mm, and a diameter of 6.4 mm. The as-cast surface finish of samples was considered to be sufficiently accurate to

avoid machining, and only some excess flash along the parting line of the die was manually removed.

The tensile test specimens were solution heat treated in an electric-resistance heated-air-circulating box-type muffle furnace at 475 °C or 525 °C for 15, 60, 240, and 480 minutes (including the heat-up time of the specimens) and immediately quenched in water at room temperature. The temperature of the electric furnace was set; when it was stable for at least 30 minutes, the tensile specimens were inserted inside the furnace. For each solution temperature, a batch of specimens was placed into the furnace in a steel frame, in order to provide a close-to-equivalent heating-up rate in each experiment. While some samples were tensile tested in the as-quenched (AQ) condition, other specimens were artificially aged at 170 °C for 8 hours after solutionizing and water quenching (T6). Additional specimens were tested in the T1 condition. While the AQ specimens were stored for 1 day in a freezer (at approximately -18 °C) before conducting the tensile test, the T6-treated specimens were immediately tested.

The tensile tests were done on an MTS 880 tensile testing machine (MTS Co., Eden Prairie, MN). The crosshead speed used was 2 mm/min ( $\dot{\epsilon} \sim 10^{-3} s^{-1}$ ). The strain was measured using a 25-mm extensometer. Two or more specimens were tested for each condition. When the experimental data differed by more than 5 pct, another tensile specimen was tested.

Microhardness measurements were performed on ground and polished samples cut from the gage sections of cylindrical test bars. The samples were stored a standard 30 days at ~25 °C, to stabilize mechanical properties by room-temperature aging (T4 condition). Vickers microhardness measurements were carried out using loads of 0.05 and 0.005 kgf and a 30-second dwell period, according to the standard ASTM E-384. The measurements were done at eight different locations over the cross section of the sample; the typical standard deviation was 5 HV.

The samples cut from the cross section of the gage length were mechanically prepared to a 1- $\mu$ m finish with diamond paste and, finally, polished with a commercial fine silica slurry (Struers OP-S, Struers A/S, Ballerup, Denmark) for metallographic investigations. Microstructural analysis was carried out using an optical microscope and a scanning electron microscope (SEM) equipped with an energy-dispersive spectrometer (EDS), and quantitatively analyzed using an image analyzer (Kontron KS300, Kontron Elektronik GmbH, Munich, Germany). To quantify the microstructural changes during solution heat treatment, the image analysis was focused on the size, aspect ratio, and interparticle spacing of the eutectic silicon particles. Size is defined as the equivalent circle diameter ( $d$ ); the aspect ratio ( $\alpha$ ) is the ratio of the maximum to the minimum Ferets. To obtain a statistical average of the distribution, a series of at least 15 photographs of each specimen were taken; each measurement included more than 1000 particles. The secondary phases, such as the  $Mg_2Si$  particles, and the iron-rich intermetallics were excluded from the measurements. To quantitatively calculate the eutectic area fraction in the entire cross section of tensile specimens

**Table I. Chemical Composition of the AlSi7MgMn Alloy Studied in the Present Work (Weight Percent)**

Alloy	Al	Si	Fe	Mn	Mg	Ti	Sr	B
Al7SiMg	bal	6.97	0.136	0.68	0.30	0.107	0.0280	0.0004

**Table II. Process Parameters**

Parameter (Piston)	Value
First phase velocity ( $v_1$ ) ( $ms^{-1}$ )	0.5
Filling phase velocity ( $v_2$ ) ( $ms^{-1}$ )	4.2
After pressure ( $P_3$ ) (MPa)	60

in the T1 condition, the polished specimens were etched in a modified Murakami etchant (60 mL H<sub>2</sub>O, 10 g NaOH, and 5 g K<sub>3</sub>Fe(CN)<sub>6</sub>).<sup>[27]</sup> At low magnification, the  $\alpha$ -Al phase and the Al-Si eutectic and intermetallics appeared white and black, respectively, and, therefore, distinguishable by quantitative metallography.

In order to study the damage after plastic strain and surface slip bands under various strength levels and strains, tensile test bars with a rectangular cross section were obtained from the central zone of the die-cast plates and one face was metallographically polished. The flat tensile specimens were 135-mm long, 20-mm wide, and 3-mm thick, with a gage length of 35 mm and a width of 10 mm.

Specimens in the T1 condition, as well as those solution heat treated for 15, 60, 240, and 480 minutes at 525 °C and aged 8 hours at 170 °C (T6), were strained to different displacements (usually between 1 and 7 pct). When the total engineering strain was equal to the preset value, loading was immediately stopped. The specimen was then removed and observed under an optical

microscope, using Nomarski interference contrast to reveal the slip bands.

### III. RESULTS AND DISCUSSION

#### A. Microstructural Observations

A typical macrostructure taken from the cross section of the gage length of as-die-cast samples is shown in Figure 1. The characteristic dark band follows the contour of the casting surface. Recently, Gourlay *et al.*<sup>[28]</sup> explained the formation of banded defects in solidifying high-pressure die-cast alloys, applying the principles developed for cohesionless granular materials. Partially solidified alloys in HPDC conditions, *i.e.*, under large pressures ( $\leq 100$  MPa) and with a large number of small crystals ( $\sim 10$   $\mu$ m), can exhibit the characteristics of a cohesionless granular material, including Reynolds' dilatancy and strain localization in dilatant shear bands. Generally, in die-cast Al-Si alloys, these bands contain a segregated eutectic fraction, and their position

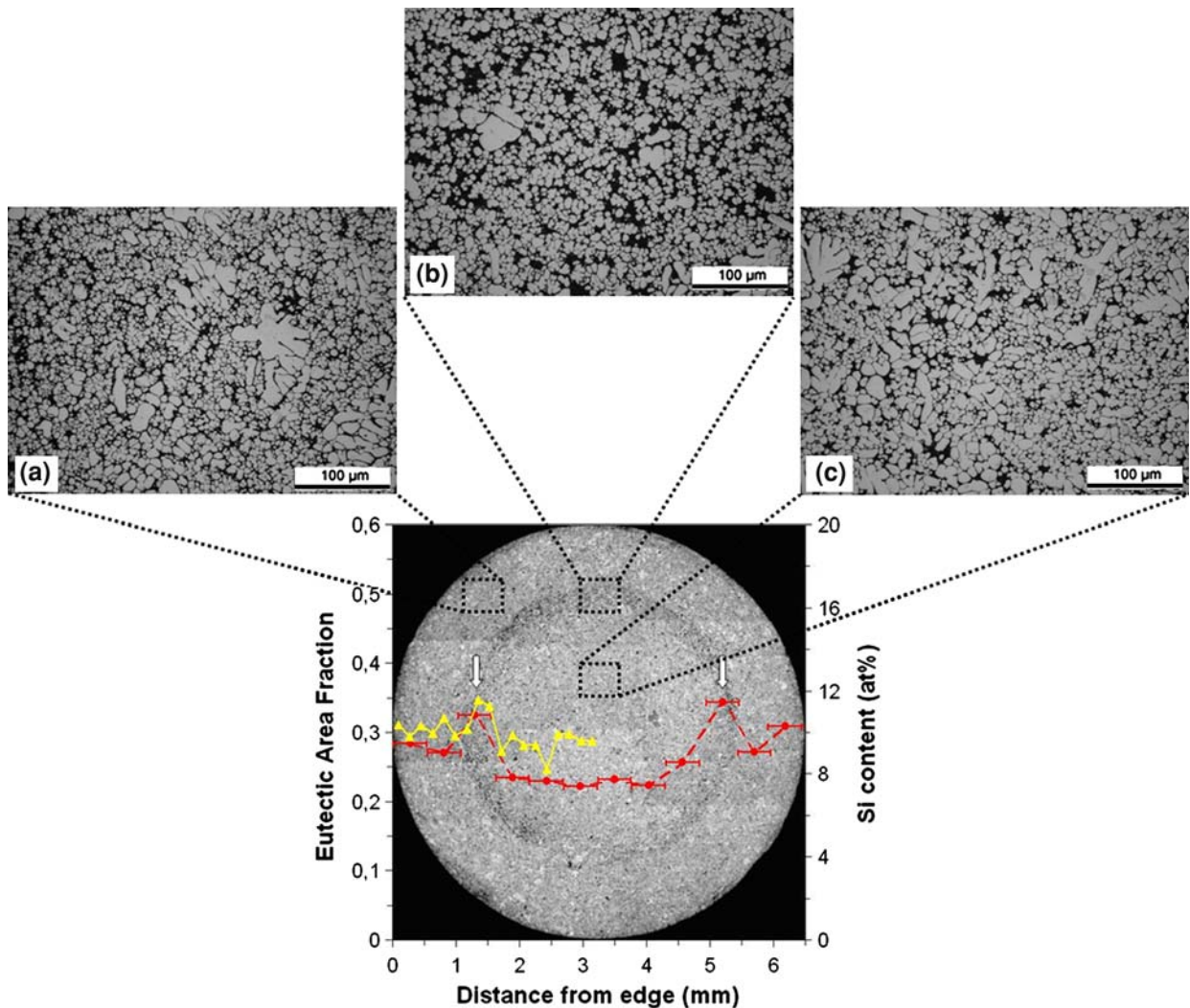


Fig. 1—Area fraction of eutectic (dashed line) and at. pct Si (solid line) over the cross section of gage length of a round tensile specimen in T1 condition. Typical microstructures obtained from different positions in the cross section are also shown. (a) Zone 1 (near the surface), (b) zone 2 (in the segregation band), and (c) zone 3 (in the central region). Arrows indicate the segregation band.

and appearance are influenced by silicon content and solidification history.<sup>[25,28,29]</sup> In order to study how the local eutectic amount varies over the cross section of as-die-cast samples, the eutectic area fraction was calculated by quantitative optical microscopy. The distribution of eutectic area fraction is overlapped to the macrostructure of a sample (Figure 1). Each data point represents the eutectic fraction in an area  $397 \times 537 \mu\text{m}$ , depicted by horizontal bars in the figure. The low eutectic area fraction, in the range of 0.25 to 0.35, can be due to the high solidification rate in HPDC; the system behaves as though the eutectic point is shifted to a higher silicon content and the eutectic temperature is depressed.<sup>[30]</sup> The average silicon composition (in atomic percent) along the radius of a cross-sectioned sample was also measured by means of EDS analysis in a SEM (FEI Quanta 400, FEI Co., Hillsboro, OR) and plotted in Figure 1. The average silicon content was calculated in an area of material  $180 \times 130 \mu\text{m}$  in size. The different techniques reflect similar results and show evidence of a peak in the region of  $\sim 1.4 \text{ mm}$  from the surface of the casting. The arrows in the figure indicate the central position of the segregation band. These findings are in agreement with the results reported in References 25, 28, and 29.

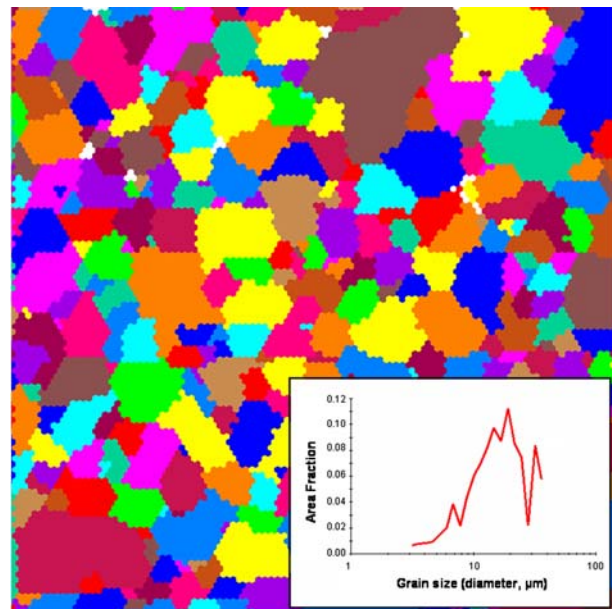
The typical microstructures obtained from different positions in the cross section of die-cast samples in the T1 condition are also shown in Figure 1. The micrographs refer to the layer near the surface of the sample, the region of the defect band, and the center of the casting; throughout this article, these three different locations will be referred to as zones 1, 2, and 3, respectively.

Externally solidified crystals (ESCs) are observed in the cross section of castings; their amounts vary along the main axis of the tensile bars. In generic die castings, a higher fraction of ESCs was observed near the gate and a lower amount was observed further from the gate.<sup>[31,32]</sup> In a study of die-cast tensile specimens,<sup>[25]</sup> it was assumed that a great fraction of ESCs did not flow into the cavity and remained in the biscuit and runner system.

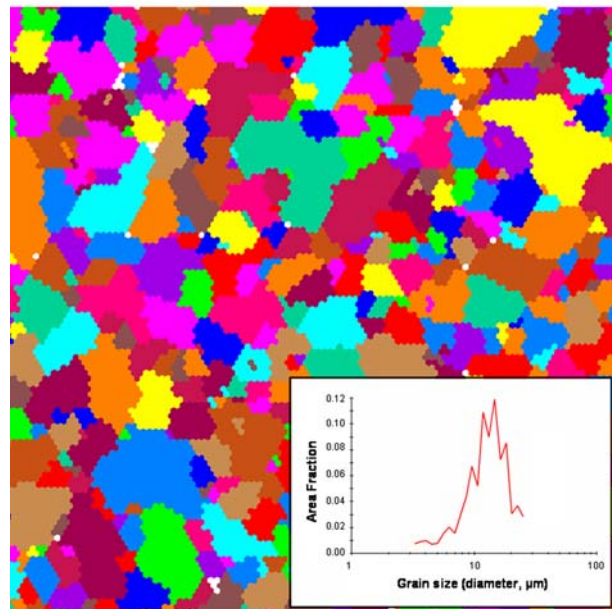
The grain size, characterized by means of the electron backscattered diffraction (EBSD) technique, is in the range of 10 to  $25 \mu\text{m}$  and the primary  $\alpha\text{-Al}$  crystals show a globular/rosette morphology. Some coarse ESCs with an elongated trunklike morphology are present. The grains observed in the central region are coarser than those in the layer near the surface of the castings (Figure 2).

As expected, the eutectic Si exhibits a fibrous morphology in the T1 condition (Figure 3). The fineness is caused by the Sr modification and the high solidification rate. It is well established that rapid solidification changes the eutectic Si shape so that it is similar to chemically modified eutectic Si.<sup>[30]</sup> The EDS analysis revealed coarser  $\alpha\text{-Al(FeMnSi)}$  intermetallic particles in the microstructure (Figure 4). The area fraction of  $\alpha\text{-Al(FeMnSi)}$  particles, calculated by quantitative optical microscopy, is similar in zones 1 and 3 ( $\sim 2.10 \text{ pct}$ ) and higher in zone 2 ( $\sim 2.90 \text{ pct}$ ).

The influence of the solution heat treatment time and temperature on the microstructure of die-cast round bars is shown in Figure 5. After 15 minutes of solution



(a)



(b)

Fig. 2—EBSD maps showing the grain size distribution (a) near the surface and (b) in the central cross section of a T1 specimen.

heat treatment at  $475 \text{ }^\circ\text{C}$ , the silicon particles become coarser and the interparticle distance increases (Figure 5(a)). Rayleigh instability<sup>[33]</sup> occurs; silicon particles undergo necking and are broken down into fragments. Due to the instability of the interfaces between the two different phases and a reduction in the total interface energy, spheroidization and coarsening processes occur. A prolonged solution treatment of 480 minutes at  $475 \text{ }^\circ\text{C}$  leads to extensive coarsening of the particles, with a small effect on the spheroidization

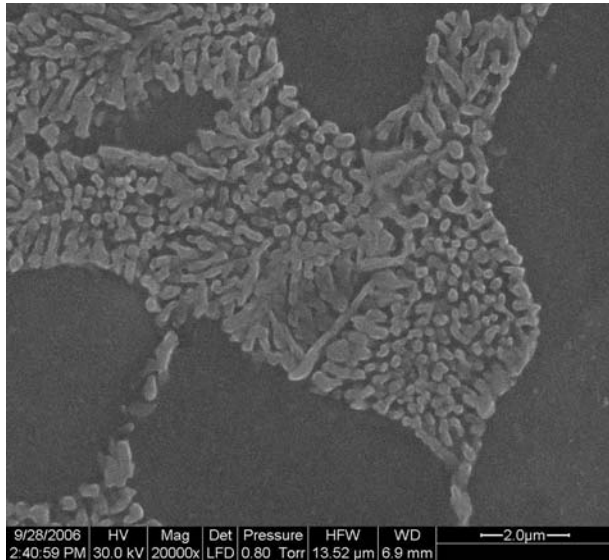


Fig. 3—Silicon crystals in the eutectic region of die-cast AlSi7MgMn alloy in T1 condition. SEM micrograph in lightly etched condition.

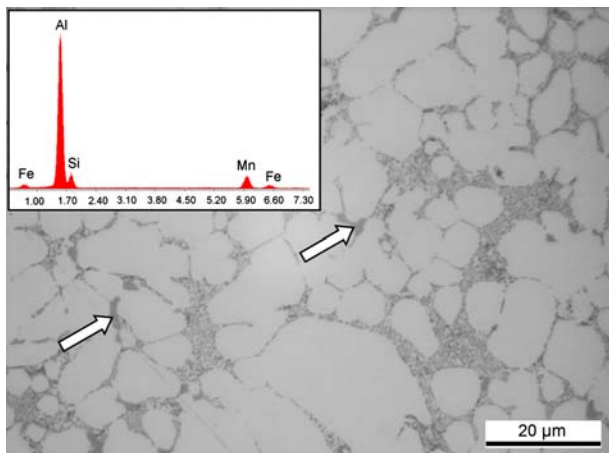


Fig. 4—Microstructure of die-cast AlSi7MgMn alloy taken from zone 1 of a round tensile specimen in T1 condition. Arrows indicate  $\alpha$ -Al(FeMnSi) intermetallic particles, as revealed by EDS spectra.

level (Figure 5(b)). The interparticle spacing increases significantly. Because the coarsening and spheroidization are diffusion-controlled processes, they are directly proportional to the solution temperature. In the present investigation, the heat treatment at 525 °C leads to coarser silicon than does the heat treatment at 475 °C, for every given solution time (Figures 5(c) and (d)). Table III shows how  $\alpha$ -Al(FeMnSi) intermetallic particles are not significantly affected by the solution heat treatment in the range of time and temperature used in the present work, in accordance with Reference 34.

As demonstrated by Lumley *et al.*,<sup>[7-9]</sup> surface blistering and discoloration of HPDC components diminish when the solution heat treatment time is reduced or the temperature lowered. Moreover, unacceptable distortions or cracking of complex-shaped castings can be controlled. In the present work, only the tensile test specimens solution treated 240 and 480 minutes at

525 °C showed surface blisters (only a few), while no samples experienced significant dimensional distortions, which is reasonable to expect from their geometry.

Figures 6(a) and (b) show the quantitative variation in the average Si particle diameter and the average aspect ratio as a function of solution time at 475 °C and 525 °C. The point zero in the time axis represents the T1 condition. The analysis is focused in zones 1 and 2. Generally, the average diameter of silicon particles increases rapidly within the first 15 minutes at the solution temperature. They then increase slowly with increasing solution time. As previously observed, an increased solution heat treatment temperature results in the increased diffusivity of Si and, therefore, a rapid coarsening mechanism; the dissolution of small particles, however, leads to the growth of larger ones.<sup>[35]</sup> While Si particles show a similar size in the region near the surface and in the central zone of tensile bars, the highest silicon concentration (~12 at. pct) in the region of segregation band leads to coarser silicon particles. Thus, the final microstructure will display a layered structure, with a different coarseness level in the distinct zones of the casting.

The typical growth rates for gravity die castings have been estimated to be in the range of 0.02 to 0.07  $\mu\text{m}/\text{h}$ . Silicon growth takes place according to the ordinary Lifshitz-Slyozov-Wagner equation:<sup>[36]</sup>

$$R^3 - R_0^3 = \frac{8DC_0\gamma V^2}{9R_{\text{gas}}T}t \quad [1]$$

where  $T$  and  $t$  are the temperature and time, respectively;  $R$  is the radius of the particle;  $R_0$  is the initial radius at  $t = 0$ ;  $R_{\text{gas}}$  is the gas constant;  $V$  is the molar volume;  $C_0$  is the equilibrium concentration of structures in matrix;  $\gamma$  is the surface energy of the particle; and  $D$  is the diffusion coefficient.<sup>[36]</sup> In the present work, this relationship has been estimated by regression analysis, through which the equivalent diameter was transformed into the equivalent radius and a linear regression analysis was carried out with respect to  $t^{1/3}$ , using the coefficient of the determination  $R^2$  to evaluate the quality of the least-squares fitting (Figure 7). When  $R^2$  is equal to 1, the fit is perfect. As can be observed in Figure 7, the fit is good for any solution temperature and at every position in the cross section of samples.

Up to 15 minutes of solution heat treatment, there is a rapid decrease in the aspect ratio of the Si particles. The decrease is approximately 16 and 19 pct at solutionizing temperatures of 475 °C and 525 °C, respectively. By increasing the solutionizing time from 15 to 480 minutes, there is a relatively small decrease in the aspect ratio (~5 pct), independent of the solution temperature. The average aspect ratio values are steady in the range of 1.4 to 1.5, indicating a good spheroidization level supporting the micrographs in Figure 5. This demonstrates that a higher solutionizing temperature promotes the spheroidization of eutectic Si, but also that solution heat treatments beyond 15 minutes at the investigated temperature have a minor effect on the extent of spheroidization. Generally, the aspect ratios in zones 1 and 2 are quite similar.

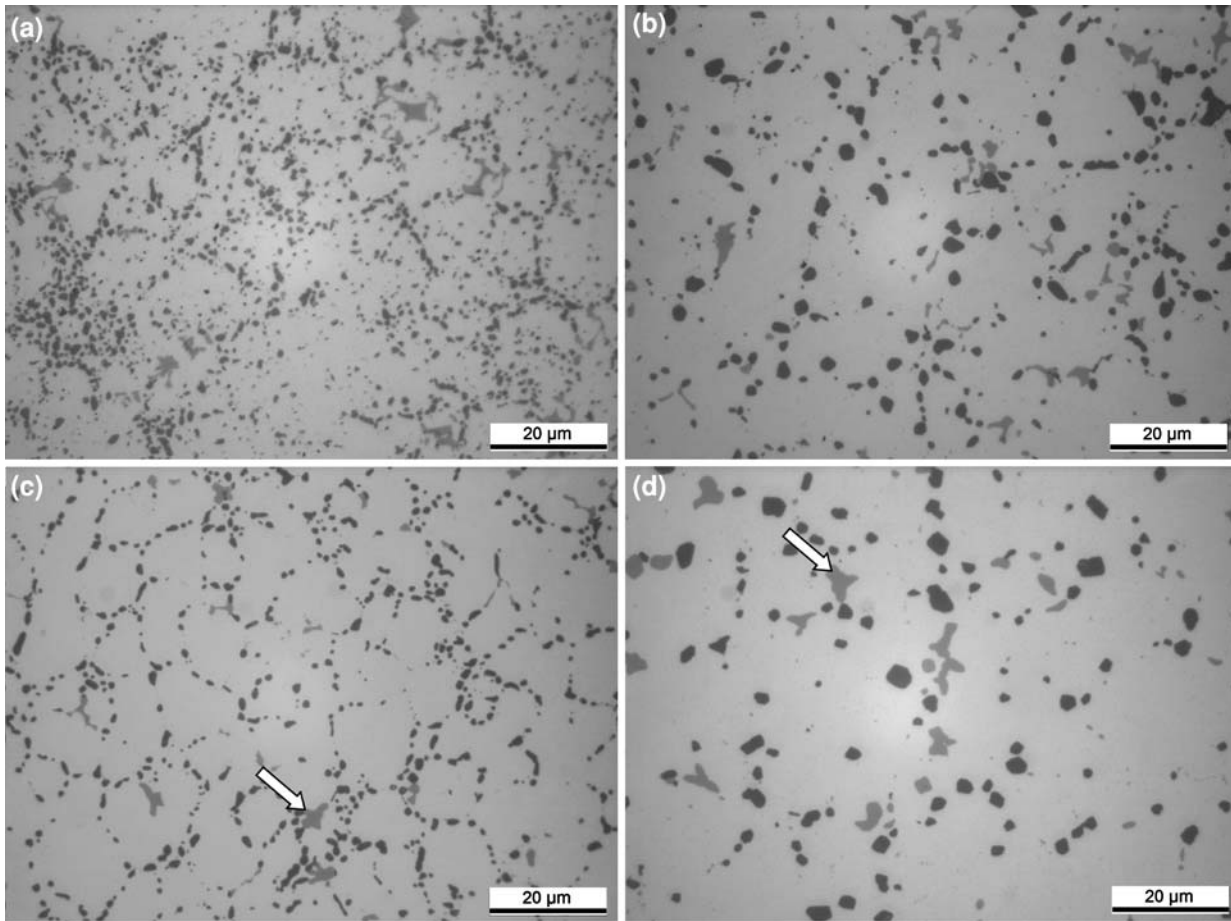


Fig. 5—Microstructure of die-cast AlSi7MgMn alloy after solution heat treatment. The alloy have been solutionized at 475 °C for (a) 15 min and (b) 480 min, at 525 °C for (c) 15 min and (d) 480 min. Arrows indicate  $\alpha$ -Al(FeMnSi) intermetallic particles.

**Table III. Average Diameter ( $d$ ) of  $\alpha$ -Al(FeMnSi) Intermetallic Particles as a Function of the Solution Heat Treatment Time at 475 °C and 525 °C (Standard Deviation in Parentheses); Data Refer to Zones 1 and 2**

Location	Temperature (°C)	T1 Condition	Time of Solution Heat Treatment (Min)			
			15	60	240	480
Zone 1	475 °C	1.92 (0.89)	1.77 (0.98)	1.88 (0.94)	1.78 (1.04)	1.97 (0.98)
	525 °C		1.97 (1.10)	1.82 (1.21)	1.90 (1.30)	1.97 (1.13)
Zone 2	475 °C	2.90 (1.60)	2.85 (1.66)	2.80 (1.57)	2.70 (1.68)	2.88 (1.57)
	525 °C		2.80 (1.47)	2.71 (1.58)	2.49 (1.54)	2.67 (1.53)

Figures 8(a) and (b) show the distribution of Si particles in zone 1 as a function of the combined parameter  $\alpha d$  for samples heat treated at various temperatures and times. Cáceres *et al.*<sup>[20]</sup> demonstrated that the eutectic Si particles in AlSiMg gravity-cast alloys crack progressively with increasing applied plastic deformation, and that the crack is favorable for the larger and longer particles, even if the progression of particle cracking is more gradual in a finer microstructure. In addition, it was observed that the population of cracked particles is distributed according to the  $\alpha d$  parameter and is characterized by its average  $\alpha d$  value. In the present work, the particles undergo great changes

in  $\alpha d$  distribution after short times (15 minutes) of solution heat treatment; the fraction of particles with a smaller  $\alpha d$  parameter is immediately reduced, while the number of particles with a greater  $\alpha d$  parameter is increased. Similar changes in particle distribution are not observed by increasing the solution times, even if the distribution curves flatten with solution time and their peaks move to the right toward higher  $\alpha d$  values. A comparison of the effect of temperature shows significant differences in the distribution of the particles. For a given solution treatment time, increasing the solution temperature from 475 °C to 525 °C clearly increases the fraction of Si particles with higher  $\alpha d$  values.

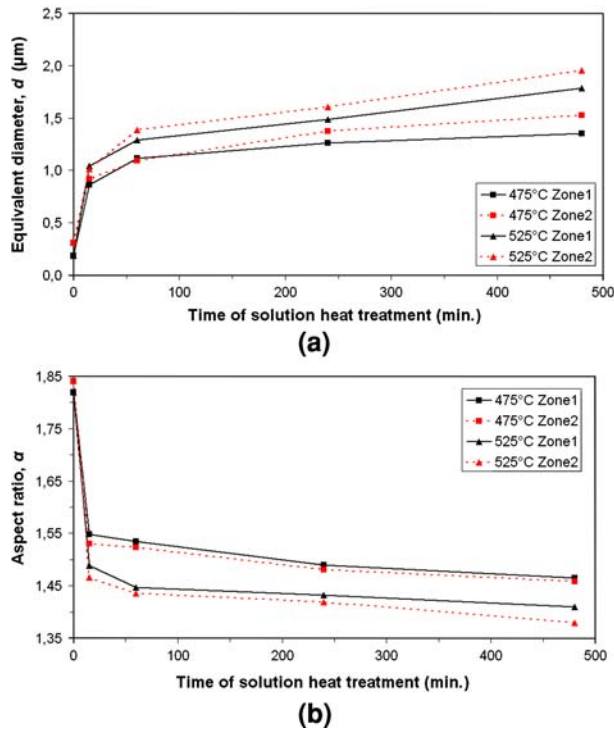


Fig. 6—(a) Average diameter and (b) aspect ratio of the eutectic Si particles as a function of solution heat treatment time at 475 °C and 525 °C. Data refer to zones 1 and 2.

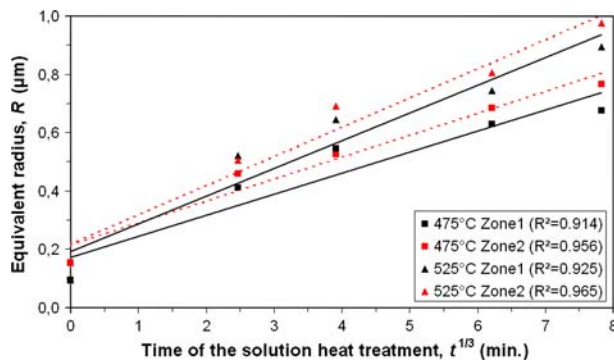


Fig. 7—Linear regression analysis of eutectic Si equivalent radius with  $t^{1/3}$ ; coefficients of determination,  $R^2$ , are given. The analysis is carried in zones 1 and 2.

The distribution of silicon particles in the segregation band reflects behavior similar to that shown in Figure 8. Comparing the results with those obtained in zone 1, the distribution curves of the Si particles in zone 2 as a function of the parameter  $\alpha d$  for samples heat treated at various temperatures and times shift to higher  $\alpha d$  values. This can be explained by the eutectic Si behavior. Because the Si particles in zone 2 show aspect ratio values similar to those obtained in zone 1 but with a higher average diameter (Figure 6), the final result is the increment of the combined parameter  $\alpha d$ .

In the present work, the mean  $\alpha d$  value of the particles in zones 1 and 3 increases from  $\sim 0.36 \mu\text{m}$  in the T1

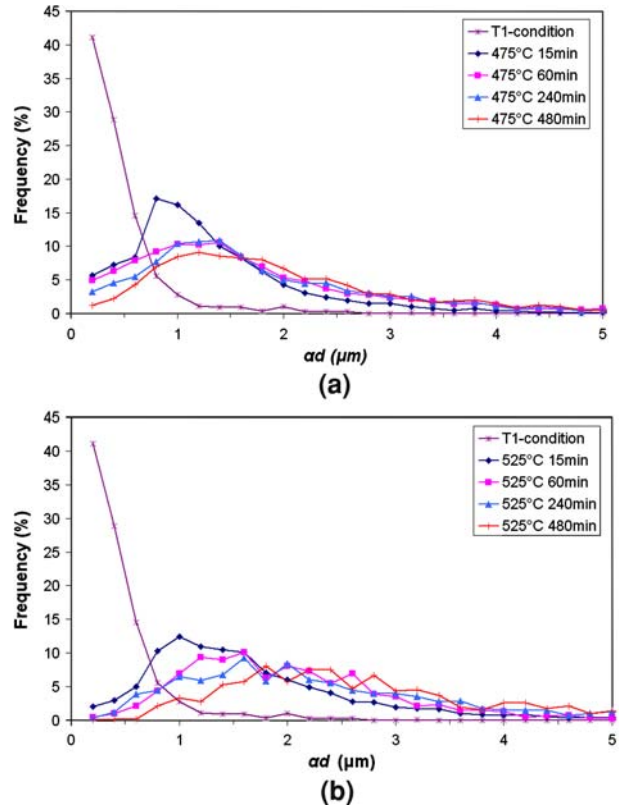


Fig. 8—Frequency distribution of the combined parameter  $\alpha d$  for eutectic silicon particles in zone 1. Data refer to solution heat treatments at (a) 475 °C and (b) 525 °C for different times.

specimens to  $\sim 1.36$  and  $\sim 2.07 \mu\text{m}$  in the specimens heat treated at 475 °C for 15 and 480 minutes, respectively. In zone 2, the increment in the  $\alpha d$  value is more than 130 pct in the first 15 minutes, but is only 57 pct when the solution treatment is extended up to 480 minutes. The mean  $\alpha d$  value is a function of the  $\alpha d$  distribution and, because the distribution curves in zone 2 shift to higher  $\alpha d$  values, the average  $\alpha d$  parameter increases. In addition, the  $\alpha d$  variable is a dimensional/morphological parameter, made by the combination of the size and the aspect ratio of silicon particles, *i.e.*, two parameters that show different behaviors with solution temperature and time (Figure 6). In general, a higher solution temperature increases the average  $\alpha d$  parameter by more than 15 pct. Thus, it is reasonable to expect that the cracks initiate within the segregation bands in which the mean  $\alpha d$  value of Si crystals is higher and coarser intermetallics<sup>[25]</sup> are observed; the fracture then propagates in the adjacent zones 1 and 3 following a “path” of cracked finer silicon and intermetallic particles.

The measured changes of the average interparticle spacing ( $\lambda$ ) in zones 1 and 2 during solution heat treatment at 475 °C and 525 °C are observed in Figures 9(a) and (b), respectively. In the present work, the mean ratio of the Si-particle spacing to the equivalent particle diameter ( $\lambda/d$ ) is also considered. Both of these parameters increase with increasing solution heat treatment time or temperature, in all the examined

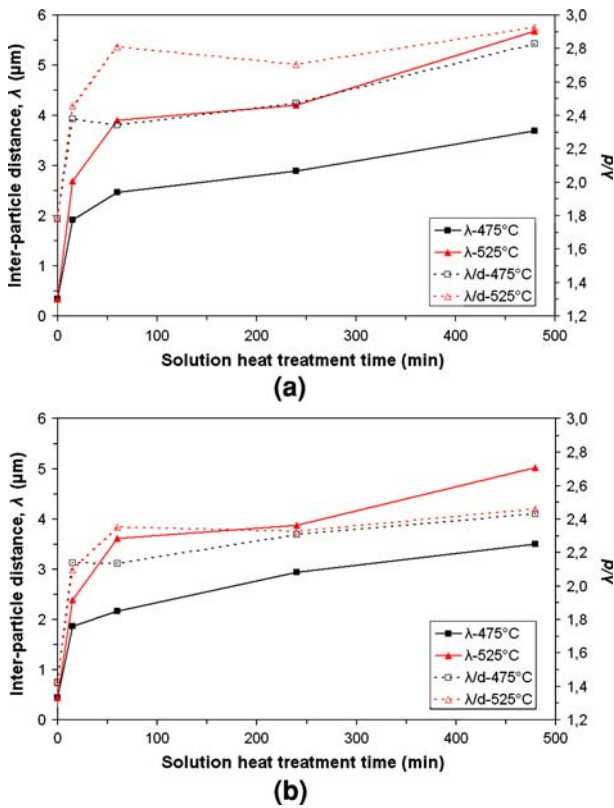


Fig. 9—Variation in average interparticle spacing ( $\lambda$ ) and the combined parameter  $\lambda/d$  of eutectic silicon particles after solution treatment at different temperatures and times. Data refer to (a) zone 1 and (b) zone 2.

locations of the specimens. The great increase within the first 15 minutes at the solution temperature of the interparticle distance confirms that the small particles are dissolved rapidly. The reduction in the interparticle spacing with increasing Si content in the segregation band is observed in the present work. This is consistent with data reported in Reference 37, in which, for gravity-cast Al-Si alloys at any one time of heat treatment, the interparticle distances diminished with increasing Si content and increased as the solutionizing time proceeded.

The  $\lambda/d$  parameter considers the combined effect of increasing interparticle spacing and coarsening of neighboring Si particles with solutionizing temperature and time. Particles with small  $\lambda/d$  values are characterized by a higher aspect ratio and fibrous morphology. Thus, high stress concentration in the  $\alpha$ -Al matrix around the particles is expected, as is the linking of voids nucleated at Si particles, which occurs at a low strain. In contrast, the increase in the  $\lambda/d$  parameter is associated with globular Si particles, so that a low stress concentration in the matrix and a better load-carrying capacity occurs after the void initiation.<sup>[17,19,20]</sup>

To investigate the influence of the amount, size, and shape of eutectic Si on the variation in hardness, Vickers microhardness measurements were completed on samples in the T1 and T4 conditions. The indentations with a load of 0.005 kgf were positioned in the eutectic

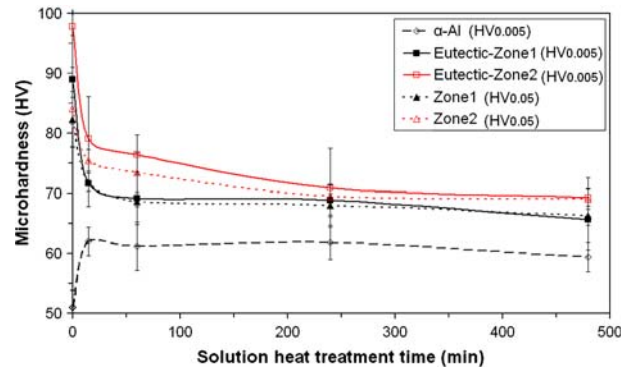


Fig. 10—Vickers microhardness measured in zones 1 and 2 of samples solution heat treated at 475 °C for different times. The microhardness was measured in the  $\alpha$ -Al crystals, the Al-Si eutectic, and at large, in zones 1 and 2. Data refer to T4 specimens. Standard deviations are given as error bars.

regions and in the  $\alpha$ -Al crystals. A load of 0.05 kgf was used to characterize the at-large hardness of zones 1 and 2. Figure 10 shows the results from specimens solution heat treated at 475 °C for various times. In general, the microhardness is higher in the eutectic regions than in the  $\alpha$ -Al crystals and, due to the highest eutectic fraction, the segregation band shows values that are higher than the region close to the casting surface. The microhardness of the  $\alpha$ -Al increases from  $\sim 51$  HV<sub>0.005</sub>, in the T1 condition, to  $\sim 63$  HV<sub>0.005</sub>, after 15 minutes of solution treatment in samples in the T4 condition; it remains constant with increasing solutionizing time. The profile of microhardness in  $\alpha$ -Al can be referred to the relatively high supersaturation of atoms (Mg and Si) and vacancies retained by rapid quenching, which causes rapid formation of Guinier-Preston zones; microhardness increases rapidly, attaining nearly maximum stable values in 4 or 5 days of natural aging.<sup>[38]</sup> Therefore, assuming that the Si and Mg concentrations in the eutectic Al remain constant (approximately equal to that of  $\alpha$ -Al crystals), the microhardness of zones 1 and 2 is determined by the hardness of the eutectic Si. The microhardness in the eutectic regions decreases rapidly within the first 15 minutes of solution treatment, due to the increased interparticle distance of eutectic Si. By increasing the solutionizing time, the curves referred to the eutectic regions decrease with a different gradient. The different microhardness behaviors in zones 1 and 2 support the measurements of the different coarsening level and the interparticle distance of Si particles.

Generally, by increasing the solution heat treatment temperature from 475 °C to 525 °C, the hardness in the eutectic regions and in the  $\alpha$ -Al crystals increases markedly on samples in the T4 condition; this can be explained through a consideration of the higher equilibrium concentration in the solid solution of Mg and Si at solutionizing temperatures of 525 °C.<sup>[16,22,33]</sup> In addition, the microhardness profiles in the eutectic regions and in the  $\alpha$ -Al crystals, as a function of solutionizing time, show trends similar to those shown in Figure 10, but with higher values.



## B. Tensile Testing

Figure 11 shows the mean YS, UTS, and elongation to fracture as a function of solution heat treatment times at 475 °C and 525 °C. The point zero in the time axis represents the T1 condition. The reference T1 specimens show values of 130 and 264 MPa for YS and UTS, respectively, and ~10 pct as elongation to fracture. Mechanical properties, especially ductility, are higher than traditional secondary type of HPDC alloys.<sup>[39]</sup> This can be related to two different factors: the chemical composition and the integrity of castings.<sup>[40]</sup> In addition to the modifying Sr, the low Fe content (0.14 wt pct) and the highest amount of Mn (~0.68 wt pct) avoid die soldering and provide high ductility, preventing the

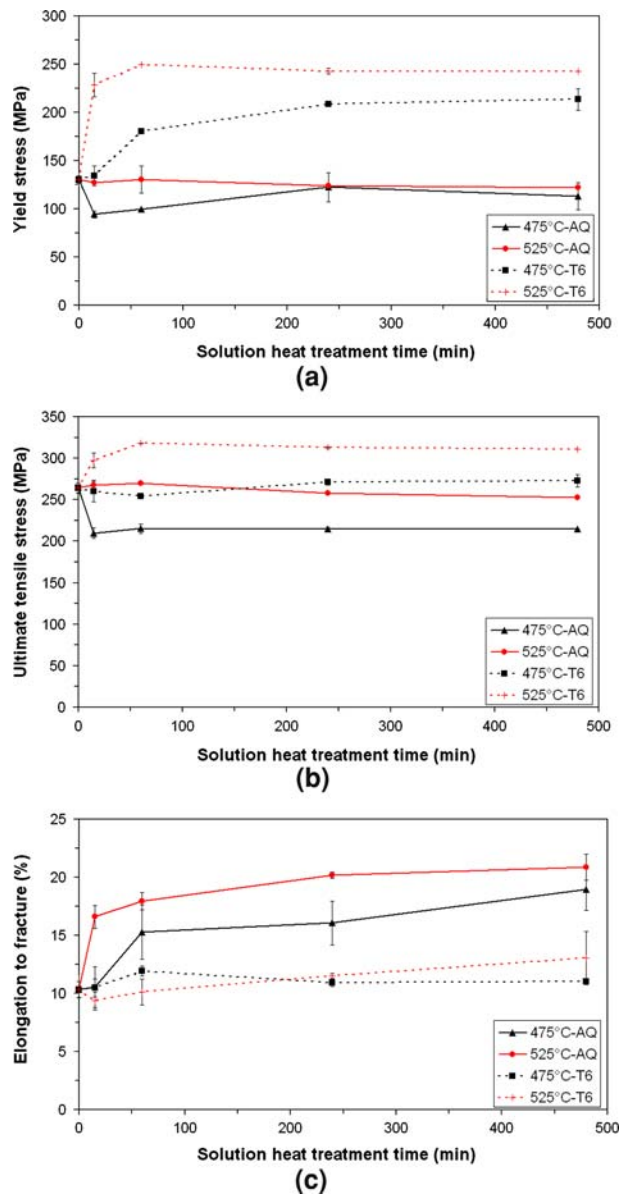


Fig. 11—Average (a) UTS, (b) YS, and (c) elongation to fracture as a function of solution treatment time at 475 °C and 525 °C. Data refer to AQ and T6 heat-treated specimens. Standard deviations are given as error bars.

formation of Fe-bearing needles. Recent work has revealed that mechanical properties of HPDC alloys can be steady when the Mn content is in the range of 0.5 to 0.8 wt pct.<sup>[24,41]</sup>

In the present work, the round tensile specimens show a good integrity level; this is reasonable to expect from their geometry and the process parameters used. A good filling behavior of the die cavity is obtained with a reduced gas entrapment and porosity size within the castings.

With a short or long solution time at 475 °C, the YS and UTS of AQ specimens are lower while at a solutionizing temperature of 525 °C; the strength is close to the as-die-cast data. In the first 15 minutes, the average elongation to fracture reaches 11 and 16 pct at 475 °C and 525 °C, respectively. With increasing solution treatment time, the average elongation to fracture increases monotonically, reaching values of 19 and 21 pct at a solution time of 480 minutes, at 475 °C and 525 °C, respectively.

Considering the T6 condition, the YS of the specimens solution treated at 475 °C slightly increases after 15 minutes. The YS increases up to 208 MPa after a solution time of 240 minutes; it is steady with extending solutionizing time. The specimens that were solution treated at 525 °C show a different YS behavior, with an increment of ~75 pct in the first 15 minutes and a maximum value (~246 MPa) reached after 60 minutes of solution heat treatment. Long solution treatment times do not affect the UTS of the alloy, as can be observed in Figure 11(b). In the first 15 minutes, the UTS of the specimens that were solution heat treated at 475 °C shows similar behavior to that of the YS property. After 60 minutes of solution heat treatment at 475 °C and 525 °C, the maximum UTS is obtained. As shown in Figure 11(c), while the average elongation to fracture of specimens solution treated at 475 °C fluctuates slightly around 11 pct, it increases monotonically up to 13 pct for a solution heat treatment of 480 minutes at 525 °C.

As expected, the improvement of strength after the controlled precipitation of small matrix-strengthening precipitates during artificial aging is consistent.<sup>[14,42]</sup> The reason for the increase in strength is primarily due to the precipitation of metastable  $\beta'$ -Mg<sub>2</sub>Si precipitates from the supersaturated solid solution, which obstructs the movement of dislocations. Generally, from the AQ condition, in which the mechanical properties are principally controlled by supersaturated solid solution, the average YS and UTS increase by more than 70 and 20 pct, respectively, in fully T6 heat-treated specimens. The impact is greater over YS, which is an essentially matrix-controlled parameter.<sup>[42]</sup> The strength and the hardness of the alloy after artificial aging increase markedly when the solid-solution temperature increases from 475 °C to 525 °C, and the different Mg and Si solubilities cannot explain this difference. It is reported that, while the maximum solubility of Mg is 0.3 and 0.5 wt pct at 475 °C and 525 °C, respectively,<sup>[16,33]</sup> the solubility of Si equals 0.7 wt pct at 475 °C and 1.1 wt pct at 525 °C.<sup>[22,33]</sup> As observed by Langsrud *et al.*<sup>[16]</sup> and Pedersen<sup>[33]</sup> for gravity-cast AlSiMg alloys, the

equilibrium solubility of vacancies, which increases exponentially with temperature, can provide the explanation. A higher quenched-in vacancy concentration probably causes a higher density of clusters of Si atoms, a more effective clustering of Si-Mg atoms, and a more efficient age hardening. The different solubilities of Si at 475 °C and 525 °C may also contribute positively.

The elongation to fracture of fully T6 heat-treated specimens is lower than that of the corresponding AQ specimens. The increment in tensile properties of T6-treated samples is accompanied by a higher number of hardening-coherent precipitates; this results in increased microstresses. This, in turn, causes lower ductility of the material, which is, moreover, influenced by the size and the morphology of the eutectic Si.<sup>[12,14,33]</sup> Zhang *et al.*,<sup>[10]</sup> Shivkumar *et al.*,<sup>[13]</sup> and Pedersen<sup>[33]</sup> showed that, in T6-treated gravity-cast aluminum alloys, there exists a region during the early stage of solution treatment in which the elongation to fracture of alloy reaches minimum values. This is due to a timing mismatch between an increase in strength and the changes in the characteristics of the Si particles.<sup>[10]</sup> In the present work, the maximum YS in the T6 condition seems to be reached after 240 and 60 minutes of solution heat treatment at 475 °C and 525 °C, respectively, and the ductility of the alloy is controlled by the features of eutectic Si, when the solution time is extended.

Similar considerations could be made for the AQ specimens. In detail, the average YS shows almost constant values (~107 and ~126 MPa at solutionizing temperatures of 475 °C and 525 °C, respectively) independently from the solution heat treatment time and, therefore, the elongation to fracture continually increases, due to the size and morphological changes of the Si particles.

Figures 12 and 13 illustrate the interaction between the fracture path and the  $\alpha$ -Al grain boundaries. The  $\alpha$ -Al globules are defined by a high density of Si particles (Figure 3). In T1 specimens, the grain size is in the range

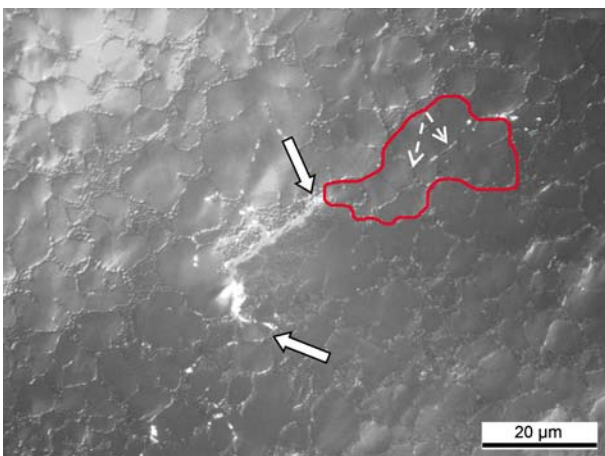


Fig. 12—Nomarski interference-contrast micrograph showing the interaction between crack path and grain boundaries (identified by the arrows) in a T1 specimen. A grain is marked up with a continuous red line, while the dashed arrows mark the lines separating the  $\alpha$ -Al cells. Applied strain is 7.1 pct.

of 10 to 25  $\mu\text{m}$  and the  $\alpha$ -Al globules show similar or lower dimensions (Figure 12). The grain boundaries are obstacles to slip (Figure 12). In T6 heat-treated specimens, by increasing the solution time or temperature, the cell structure fades and does not interrupt the slip bands, which are much longer than the  $\alpha$ -Al cells. The eutectic silicon particles interact with the slip bands individually rather than collectively, as in the case of distinct cell boundaries. Therefore, the most significant obstacles to the slip bands are, again, the grain boundaries (Figure 13). The grain boundaries in Figures 12 and 13 are identified by the different directions in the slip traces under the Nomarski interference contrast, even at high-magnification observations. As demonstrated by Cáceres *et al.*<sup>[20]</sup> and Wang *et al.*,<sup>[21]</sup> the interaction between the grain boundaries and slip bands have consequences for the cracking of the eutectic Si particles during plastic straining. Brittle fracture by cleavage of the Si particles is known to start at plastic strains of about 1 to 2 pct in AlSiMg cast alloys and continuing up to final fracture.<sup>[20]</sup> Plastic incompatibility between adjacent grains and, with increasing strain, the buildup of a forest of dislocations near the grain boundaries<sup>[17,20,21]</sup> makes stress relaxation more difficult for the silicon and intermetallic particles located at or

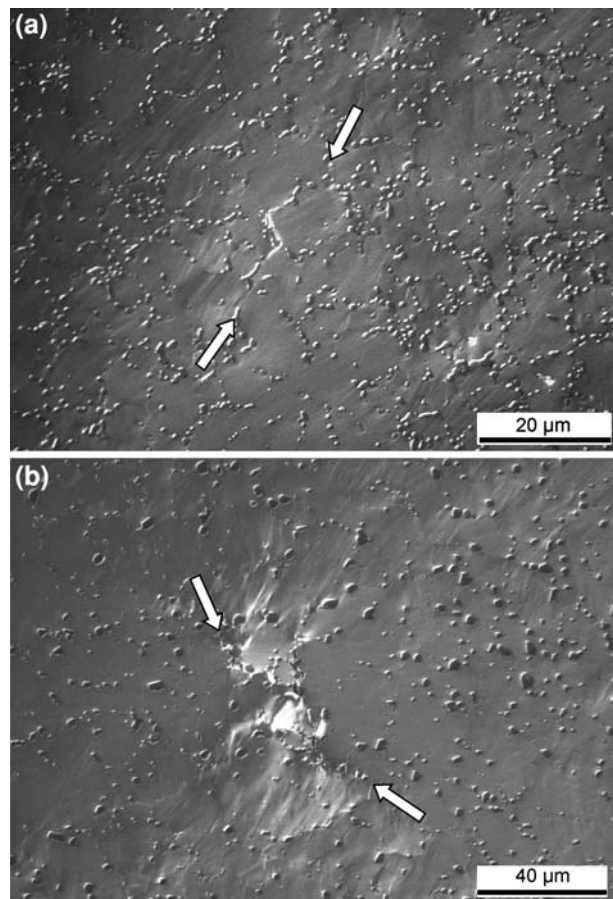


Fig. 13—Nomarski-contrast micrographs showing the interaction between crack path and grain boundaries (identified by the arrows) in samples solutionized at 525 °C for (a) 15 and (b) 480 min and aged at 170 °C for 8 h. Applied strain is 1.4 pct.

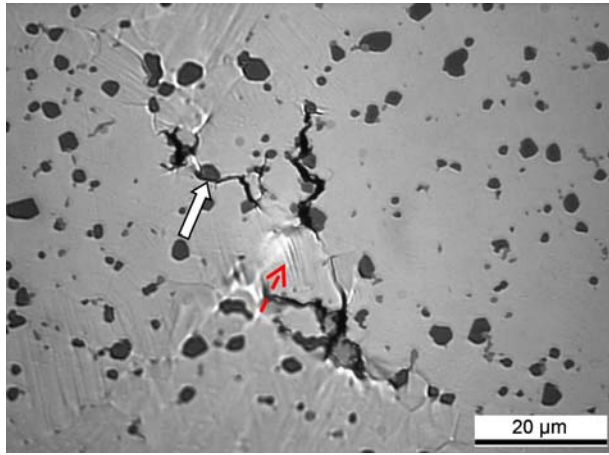


Fig. 14—Micrograph showing cracked particles in a sample deformed to 1.4 pct tensile strain, solution treated at 525 °C for 480 min and aged at 170 °C for 8 h. The arrow indicates decohesion on Al matrix/Si particle interface. The dashed arrow shows slip bands between adjacent cracks.

near the grain boundaries than for the isolated particles away from the grain boundaries. Particle stresses are, therefore, more likely to be higher near the grain boundaries, increasing the local probability of particle cracking and, consequently, favoring an intergranular type of fracture.<sup>[21]</sup>

In general, it is observed that silicon and intermetallic particle cleavage is mainly perpendicular to the loading direction and that it is easier for coarser and longer particles to crack. It has been demonstrated that the average interparticle spacing increases with the solution heat treatment time or temperature in all the examined locations of the specimens. Therefore, in heat-treated specimens, the fracture follows a path of “isolated” Si and intermetallic particles (Figure 13); in T1 specimens (Figure 12), however, the average interparticle spacing is lower. Decohesion at low strain on the Al matrix/ $\alpha$ -Al (FeMnSi) and the Al matrix/Si particle interface takes also place (Figure 14). Figure 14 shows the nucleation of cracks through the coalescence of adjacent microcracks created during the fracture of Si and intermetallic particles. Slip bands appear between adjacent cracks. As reported by Mishnaevsky *et al.*,<sup>[18]</sup> the necking along the slip bands between the microcracks is the main mechanism for their coalescence, and the microcrack coalescence is the origin of the reduction of the load-bearing area. Microcrack coalescence is observed only after slip bands have formed between them and not due to their expansion or growth.

#### IV. CONCLUSIONS

The effect of solution heat treatment time and temperature on the microstructure, tensile properties, and mode of fracture of a high-pressure die-cast AlSi7MgMn has been investigated. Based on the results obtained in the present study, the following conclusions can be drawn.

1. A solution heat treatment of 15 minutes at 475 °C, or a heat treatment involving even more time at 525 °C, causes spheroidization, coarsening, and an increase in the interparticle distance of the eutectic silicon particles, leading to substantial changes in the microstructure and mechanical properties.
2. The distribution of the combined parameter  $\alpha d$  of silicon particles is significantly affected by a short solution heat treatment time. The fraction of eutectic Si with a smaller  $\alpha d$  parameter is immediately reduced after a solution treatment of 15 minutes, while the number of particles with a greater  $\alpha d$  parameter is increased. Similar changes in particle distribution are not observed by increasing solution times.
3. Considering the AQ condition, with either a short or a long solution time at 475 °C, the YS and UTS are lower than the as-die-cast values; at a solution temperature of 525 °C, however, the strength is close to the T1 data. With an increasing solution treatment temperature or time, the average elongation to fracture increases monotonically.
4. In the T6 condition, the YS reaches its maximum at 240 and 60 minutes of solution treatment at 475 °C and 525 °C, respectively. Long solution treatment times do not affect the UTS of the alloy. The improvement of strength after the controlled precipitation of small matrix-strengthening precipitates during artificial aging is consistent.
5. From the AQ condition, in which the tensile properties are principally controlled by supersaturated solid solution, the average YS and UTS increase by more than 70 and 20 pct, respectively, in a fully T6 heat-treated condition. The impact is greater over the YS, which is an essentially matrix-controlled parameter.
6. The strength and the hardness of the alloy after artificial aging increase markedly when the solutionizing temperature increases from 475 °C to 525 °C.
7. The ductility of the T6 heat-treated alloy is determined by both the size and morphology of the eutectic silicon crystals and the effect of precipitation hardening.
8. The fracture mode is predominantly intergranular in the T1 and T6 conditions.

#### ACKNOWLEDGMENTS

This work was developed within the Marie Curie Training Sites Project (Fellowship Contract No. HPMT-CT-2001-00305), supported by the European Union inside the Human Potential Programme–5th FW Programme.

#### REFERENCES

1. A.C. Street: *The Die Casting Book*, 2nd ed., Portcullis Press Ltd., Redhill, Surrey, 1986, pp. 3–655.
2. L. Andreoni, M. Case, and G. Pomesano: *Quaderni della Colata a Pressione delle Leghe di Alluminio*, Edimet, Brescia, 1995, pp. 5–68.

3. E.J. Vinarcik: *High Integrity Die Casting Processes*, John Wiley & Sons, New York, NY.
4. D. Apelian and M.M. Makhlof: *High Integrity Aluminium Die Casting: Alloys, Processes and Melt Preparation*, North American Die Casting Association, Des Plaines, IL, 2004, pp. 1–14.
5. C.H. Cáceres and B.I. Selling: *Mater. Sci. Eng. A*, 1996, vol. 220, pp. 109–16.
6. X. Dai, X. Yang, J. Campbell, and J. Wood: *Mater. Sci. Technol.*, 2004, vol. 20, pp. 505–13.
7. R.N. Lumley, R.G. O'Donnell, D.R. Gunasegaram, and M. Givord: *Mater. Sci. Forum*, 2006, vols. 519–521, pp. 351–58.
8. R.N. Lumley, R.G. O'Donnell, D.R. Gunasegaram, and M. Givord: *Metall. Mater. Trans. A*, 2007, vol. 38A, pp. 2564–74.
9. R.N. Lumley, R.G. O'Donnell, D.R. Gunasegaram, and M. Givord: International Patent Application PCT/2005/001909.
10. D.L. Zhang, L.H. Zheng, and D.H. StJohn: *J. Light Met.*, 2002, vol. 2, pp. 27–36.
11. P.A. Rometsch, L. Arnberg, and D.L. Zhang: *Int. J. Cast Met. Res.*, 1999, vol. 12, pp. 1–8.
12. L. Pedersen and L. Arnberg: *Metall. Mater. Trans. A*, 2001, vol. 32A, pp. 525–32.
13. S. Shivkumar, S. Ricci, C. Keller, and D. Apelian: *J. Heat Treatment*, 1990, vol. 8, pp. 63–70.
14. D.K. Dwivedi, R. Sharma, and A. Kumar: *Int. J. Cast Met. Res.*, 2006, vol. 19, pp. 275–82.
15. J.A. Taylor, D.H. StJohn, J. Barresi, and M.J. Couper: *Mater. Sci. Forum*, 2000, vol. 331, pp. 277–82.
16. Y. Langsrud and S. Brusethaug: *ICAA6*, 1998, vol. 2, pp. 733–38.
17. J.-W. Yeh and W.-P. Liu: *Metall. Mater. Trans. A*, 1996, vol. 27A, pp. 3558–68.
18. L.L. Mishnaevsky, Jr., N. Lippmann, S. Schmauder, and P. Gumbsch: *Eng. Fract. Mech.*, 1999, vol. 63, pp. 395–411.
19. C.H. Cáceres, C.J. Davidson, and J.R. Griffiths: *Mater. Sci. Eng., A*, 1995, vol. 197, pp. 171–79.
20. C.H. Cáceres and J.R. Griffiths: *Acta Mater.*, 1996, vol. 44, pp. 25–33.
21. Q.G. Wang and C.H. Cáceres: *Mater. Sci. Eng., A*, 1998, vol. 241, pp. 72–82.
22. A.L. Dons, E.K. Jensen, Y. Langsrud, E. Tromborg, and S. Brusethaug: *Metall. Mater. Trans. A*, 1999, vol. 30A, pp. 2135–46.
23. S. Seifeddine, T. Sjögren, and I.L. Svensson: *Proc. High Tech Die Casting*, AIM, Vicenza, 2006, paper no. 15.
24. A. Zovi and F. Casarotto: *Metall. Ital.*, 2007, vol. 6, pp. 33–38.
25. H.I. Laukli, C.M. Gourlay, A.K. Dahle, and O. Lohne: *Mater. Sci. Eng., A*, 2005, vols. 413–414, pp. 92–97.
26. M.C. Srivastava, O. Lohne, L. Arnberg, H.I. Laukli, and H. Gjestland: *Proc. High Tech Die Casting*, AIM, Vicenza, 2006, paper no. 10.
27. G.F. Vander Voort: *Metallography Principles and Practise*, McGraw-Hill, New York, NY, 1984, p. 612.
28. C.M. Gourlay and A.K. Dahle: *Nature*, 2007, vol. 445, pp. 70–73.
29. C.M. Gourlay, H.I. Laukli, and A.K. Dahle: *Metall. Mater. Trans. A*, 2004, vol. 35A, pp. 2881–91.
30. M.M. Makhlof and H.V. Guthy: *J. Light Met.*, 2001, vol. 1, pp. 199–218.
31. H.I. Laukli, C.M. Gourlay, and A.K. Dahle: *Metall. Mater. Trans. A*, 2005, vol. 36A, pp. 805–18.
32. H.I. Laukli, L. Arnberg, and O. Lohne: *Int. J. Cast Met. Res.*, 2005, vol. 18, pp. 65–72.
33. L. Pedersen: Doctoral Thesis, Norwegian University of Science and Technology, Trondheim, Norway, 1999.
34. L. Anantha Narayanan, F.H. Samuel, and J.E. Gruzleski: *Metall. Mater. Trans. A*, 1995, vol. 26A, pp. 2161–74.
35. G.W. Greenwood: *Acta Metall.*, 1956, vol. 4, pp. 243–48.
36. I.M. Lifshitz and V.V. Sloyozov: *J. Phys. Chem. Solids*, 1961, vol. 19, pp. 35–47.
37. F.N. Rhines and M. Aballe: *Metall. Trans. A*, 1986, vol. 17A, pp. 2139–52.
38. *ASM Handbook: Heat Treating*, vol. 4, ASM INTERNATIONAL, Materials Park, OH, 1991, p. 860.
39. M.M. Makhlof, D. Apelian, and L. Wang: *Microstructure and Properties of Aluminium Die Casting Alloys*, North American Die Casting Association, Rosemont, IL, 1998, pp. 19–91.
40. H.I. Laukli and S. Brusethaug: *Giessereiforschung*, 2007, vol. 59, pp. 16–21.
41. R. Franke, D. Dragulin, A. Zovi, and F. Casarotto: *Metall. Ital.*, 2007, vol. 5, pp. 21–26.
42. J.A. Taylor, D.H. St. John, J. Barresi, and M.J. Couper: *Int. J. Cast Met. Res.*, 2000, vol. 12, pp. 419–30.